


# Layer-dependent local gate response in graphene-supported $TaSe_2$ films studied by gate-tunable STM

Kefan Wu(吴可凡), Linfei Li(李林飞), Zhixuan Li(李志轩), Ke Zhu(祝轲), Jiayi Wang(王嘉翌), Hui Guo(郭辉), Shiyu Zhu(朱诗雨), Xiao Lin(林晓), and Hong-Jun Gao(高鸿钧)

**Citation:**Chin. Phys. B, 2026, 35 (**8**): 086802. DOI: 10.1088/1674-1056/ae66dd
http://cpb.iphy.ac.cn; http://iopscience.iop.org/cpb

**What follows is a list of articles you may be interested in**

---

## Cascade of low-energy surface phonon modes on the B-terminated $EuB_6$ surface

Yumeng Li(李雨萌), Meng Li(李萌), Lijing Huang(黄丽静), Haitao Yang(杨海涛), Hongqin Xiao(肖洪钦), Yuxuan He(何昱萱), Geng Li(李更), and Hong-Jun Gao(高鸿钧)

Chin. Phys. B, 2026, 35 (**7**): 076801. DOI: 10.1088/1674-1056/ae6568

## Spectroscopic studies of two-dimensional superconductivity

Qiang-Jun Cheng(程强军), Xu-Cun Ma(马旭村), Qi-Kun Xue(薛其坤), and Can-Li Song(宋灿立)

Chin. Phys. B, 2026, 35 (**6**): 066801. DOI: 10.1088/1674-1056/ae4c6d

## Formation of crystalline $Si_9C_{15}$ nano-islands and $Si_9C_{15}$/graphene heterostructures on Ru(0001)

Lijing Huang(黄丽静), Yumeng Li(李雨萌), Hongqin Xiao(肖洪钦), Yuxuan He(何昱萱), Geng Li(李更), and Hong-Jun Gao(高鸿钧)

Chin. Phys. B, 2026, 35 (**5**): 056801. DOI: 10.1088/1674-1056/ae4c6f

## Real-time four-dimensional scanning transmission electron microscopy through sparse sampling

A W Robinson, J Wells, A Moshtaghpour, D Nicholls, C Huang, A Velazco-Torrejon, G Nicotra, A I Kirkland, and N D Browning

Chin. Phys. B, 2024, 33 (**11**): 116804. DOI: 10.1088/1674-1056/ad8a4a

## Tunable 2H-$TaSe_2$ room-temperature terahertz photodetector

Jin Wang(王瑾), Cheng Guo(郭程), Wanlong Guo(郭万龙), Lin Wang(王林), Wangzhou Shi(石旺舟), Xiaoshuang Chen(陈效双)

Chin. Phys. B, 2019, 28 (**4**): 046802. DOI: 10.1088/1674-1056/28/4/046802

---

**RAPID COMMUNICATION**

# Layer-dependent local gate response in graphene-supported $TaSe_2$ films studied by gate-tunable STM

Kefan Wu(吴可凡)[1,2,†], Linfei Li(李林飞)[2,3,†,‡], Zhixuan Li(李志轩)[1,2,†], Ke Zhu(祝轲)[2,1], Jiayi Wang(王嘉翌)[2,1], Hui Guo(郭辉)[2,1], Shiyu Zhu(朱诗雨)[2,1], Xiao Lin(林晓)[1,2,§], and Hong-Jun Gao(高鸿钧)[2,1]

[1] *School of Physical Sciences, University of Chinese Academy of Sciences, Beijing* 100190, *China*
[2] *Beijing National Laboratory for Condensed Matter Physics, Institute of Physics, Chinese Academy of Sciences, Beijing* 100190, *China*
[3] *School of Materials Science and Engineering, School of Interdisciplinary Science, Beijing Institute of Technology, Beijing* 100081, *China*

(Received 3 April 2026; revised manuscript received 23 April 2026; accepted manuscript online 30 April 2026)

Gate-tunable scanning tunnelling microscopy (STM) enables direct correlation between electrostatic gating and local electronic states in two-dimensional correlated materials. Here, we investigate $TaSe_2$ films on graphene using a home-built gate-tunable STM setup. Large-area and atomically resolved STM images reveal well-defined $TaSe_2$ islands and an ordered charge-density-wave (CDW) superstructure. Monolayer $TaSe_2$ shows spatially resolved scanning tunnelling spectroscopy (STS) features but a strongly suppressed gate response under back-gate voltages. In contrast, bilayer $TaSe_2$ exhibits a richer zero-gate electronic structure and systematic bias-dependent evolution of CDW contrast. Fixed-point gate-dependent STS in the bilayer region demonstrates clear spectral-weight redistribution and low-energy feature evolution. Our results establish a feasible gate-tunable STM protocol for $TaSe_2$/graphene heterostructures and reveal pronounced layer-dependent local gate response in correlated two-dimensional systems.

**Keywords:** gate-tunable STM, $TaSe_2$, charge-density wave, gate response

**PACS:** 68.37.Ef, 71.45.Lr, 73.20.At, 73.40.Qv

**DOI:** 10.1088/1674-1056/ae66dd **CSTR:** 32038.14.CPB.ae66dd

## 1. Introduction

Electrostatic control of low-dimensional correlated states is central to the study of quantum materials. The broader exploration of two-dimensional (2D) materials has evolved from high-symmetry systems such as graphene[1–5] and transition-metal dichalcogenides (TMDs)[6–9] to low-symmetry layered materials including black phosphorus,[10,11] $ReS_2$[12,13] and $WTe_2$.[14,15] Reduced crystal symmetry can introduce additional physical degrees of freedom and generate in-plane anisotropic transport,[16] polarization-dependent optical response,[16] and piezoelectricity.[17,18] At the same time, reduced dimensionality in layered chalcogenides can host Peierls-type instabilities,[19,20] sliding charge-density waves,[21,22] CDW-related bound states,[23] and possible topological superconductivity.[24] Recent studies on 1T-$TiSe_2$ and $WS_2$/1T-$TaS_2$ heterostructures further show that charge-density-wave order in low-dimensional chalcogenides can be efficiently perturbed by light-induced carrier redistribution and interfacial photodoping.[25,26]

Charge-density-wave physics in 1T-type dichalcogenides has been studied for decades.[27] Single-layer 1T-$TaSe_2$, a representative correlated TMD, has emerged as a particularly important case because the Star-of-David reconstruction reshapes the electronic structure into a narrow half-filled band and promotes strong local correlations.[28–31] STM/STS and photoemission studies further showed that the correlated state evolves rapidly once a second layer is added, because shifted Star-of-David stacking, interlayer registry and interlayer hopping modify both the CDW-derived orbital structure and the low-energy gap.[28,31] Relative to the weakly screened single-layer limit, added layers enhance hybridization and dielectric screening, weaken the Mott-like state and enrich the zero-bias electronic structure.[28,31–34] A related tunability has also been discussed in monolayer $VTe_2$, where external strain can modify the competition among charge-density-wave order, Mott-insulating behavior and superconducting tendency.[35]

Gate-tunable STM proves to be particularly advantageous for investigating these phenomena, as it merges the atomic-scale sensitivity of STM with the ability to exert electrostatic control independently.[36,37] Recent local-probe studies of mirror-twin boundaries, doped Mott insulators, and other gate-addressable low-dimensional systems have demonstrated that gating can redistribute low-energy spectral weight and expose microscopic response channels inaccessible to transport measurements.[38–41] For STM-compatible back-gated devices, the usable voltage range is set jointly by dielectric

[†]These authors contributed equally to this work.
[‡]Corresponding author. E-mail: lilinfei@bit.edu.cn
[§]Corresponding author. E-mail: xlin@ucas.ac.cn

© 2026 Chinese Physical Society and IOP Publishing Ltd. All rights, including for text and data mining, AI training, and similar technologies, are reserved.

geometry, gating efficiency, and tunnelling-junction stability; several-tens-of-volts operation is therefore typical, and the −50 V to +50 V range adopted here provides a stable window for comparing monolayer and bilayer $TaSe_2$. Related studies in Chinese Physics journals have expanded the material and spectroscopic basis for investigating low-dimensional correlated systems,[42–47] while electrostatic control has also been applied to nodal-line systems, layered superconductors, and van der Waals devices.[9,48–50] Nevertheless, a direct atomic-scale comparison of monolayer and bilayer $TaSe_2$ within the same gate-tunable STM platform remains lacking, despite the recurring importance of thickness-dependent electronic structures in 1T-type CDW materials and related layered chalcogenides.[51–54]

In this work, a $TaSe_2$/graphene/$SiO_2$/Si platform compatible with low-temperature gate-tunable STM is established and used to compare monolayer and bilayer $TaSe_2$ within a unified experimental geometry. The measurements proceed in three steps. First, the device architecture, sample mounting, and wiring scheme are defined. Second, the morphology and atomic-scale structure of the $TaSe_2$ film are characterized to establish a structural and spectroscopic baseline. Third, layer-resolved gate response is examined by combining linecut spectroscopy, bias-dependent mapping, and fixed-point gate-dependent STS. The results show a markedly suppressed gate response in the monolayer region but a much clearer gate-induced spectral redistribution in the bilayer region.

## 2. Experimental methods

The gate-tunable STM platform is summarized in Fig. 1. $TaSe_2$ was integrated with graphene (Fig. 1(a)) on a $SiO_2$/Si back-gate stack (Fig. 1(b)), so that the tunnelling junction and electrostatic control share one device geometry. In the measurement configuration, the sample bias $V_b$ is applied to the STM junction, whereas the back-gate voltage $V_g$ is applied through the $SiO_2$/Si substrate. This geometry allows local spectroscopy to be tracked under continuously tuned electrostatic conditions without sacrificing atomic-scale spatial resolution. All STM/STS data reported here were acquired at a base temperature of 4.7 K. In the present device, a gate voltage range of −50 V to +50 V is employed as the primary operating window. This range facilitates stable tunneling conditions and offers a representative scope for electrostatic tuning, allowing for direct comparison between monolayer and bilayer $TaSe_2$. Repeated measurements within this interval yielded reproducible spectra without obvious dielectric-breakdown features or pronounced hysteretic distortion.

A dedicated low-temperature sample-stage wiring scheme was implemented to ensure electrical isolation, mechanical stability, and compatibility with ultra-high-vacuum STM operation (Fig. 1(c)). The sample holder, sapphire insulating layer, electrodes, bonding wires, and spring-clip fixation jointly define a stable mounting configuration. As shown in Fig. 1(d), the assembled device confirms that the back-gated sample can be reliably mounted on the STM stage. This technical design is the foundation for the layer-resolved measurements discussed below.

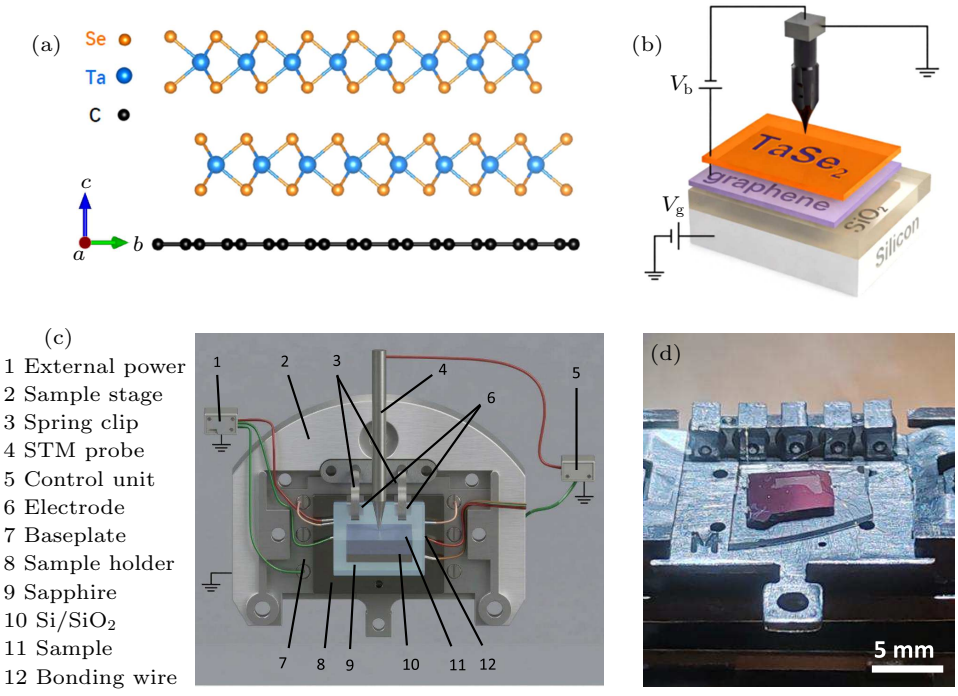



**Fig. 1.** $TaSe_2$/graphene/$SiO_2$/Si back-gated device and sample configuration for gate-tunable STM. (a) Structural model of $TaSe_2$ supported by graphene. (b) Schematic of the gate-tunable STM/STS measurement geometry, where the sample bias $V_b$ is applied to the tunnelling junction and the back-gate voltage $V_g$ tunes the carrier environment through the $SiO_2$/Si substrate. (c) Sample-stage and wiring layout used for low-temperature STM measurements. (d) Optical image of the fabricated device mounted on a sample holder.

## 3. Results and discussion

### 3.1. Surface morphology and atomic-scale structure

To clarify the structural basis for subsequent spectroscopic and gating measurements, we first characterize the surface morphology and atomic-scale structure of graphene-supported $TaSe_2$ films. The large-area STM image in Fig. 2(a) shows a well-defined $TaSe_2$ island on graphene. The coexistence of monolayer and bilayer regions within the same $TaSe_2$ island enables a clean, thickness-dependent comparison under nearly identical substrate and measurement conditions. The atomically resolved image in Fig. 2(b) reveals a Star-of-David reconstruction of $TaSe_2$ preserved on the conductive graphene support, with the FFT pattern confirming the CDW periodicity and orientation. The local magnified view in Fig. 2(c) and the representative line profile in Fig. 2(d) further verify a real-space modulation, suggesting a well-ordered correlated state with a robust real-space periodicity. These observations are consistent with a charge-density-wave-modulated surface rather than a featureless metallic background.

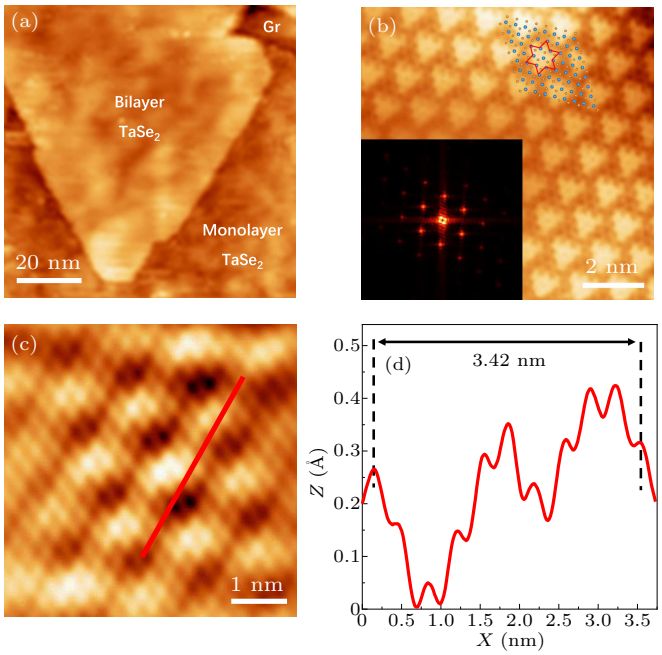



**Fig. 2.** Surface morphology and atomic-scale structural characterization of $TaSe_2$ films. (a) Large-area STM topography of the monolayer and bilayer $TaSe_2$ island grown on graphene ($V_{bias} = -2$ V, $I_{set} = 100$ pA). (b) Atomically resolved STM image showing a charge-density-wave superstructure ($V_{bias} = -1$ V, $I_{set} = 500$ pA). The overlaid guide marks the Star-of-David charge-density-wave unit, and the inset shows the corresponding fast Fourier transform pattern. (c) Local magnified STM image ($V_{bias} = -1$ V, $I_{set} = 1$ nA). (d) Line profile taken along the red line in (c).

### 3.2. Spatially resolved spectroscopy and suppressed gate response in monolayer $TaSe_2$

With the atomic-scale structural features confirmed, we next examine the local electronic states and electrostatic gating response of monolayer $TaSe_2$ to establish a thickness-comparison baseline. As shown in Fig. 3(a), the STM image marks a linecut path extending from position 1 to position 27. The corresponding $dI/dV$ spectra in Fig. 3(b) show that the local electronic structure evolves continuously along the line trace rather than remaining strictly uniform. For clarity, the valence-band (VB) and conduction-band (CB) features are marked by arrows in Figs. 3(b) and 3(d). The intensity map in Fig. 3(c) makes this behavior more transparent by displaying the redistribution of spectral weight as a joint function of position and bias.

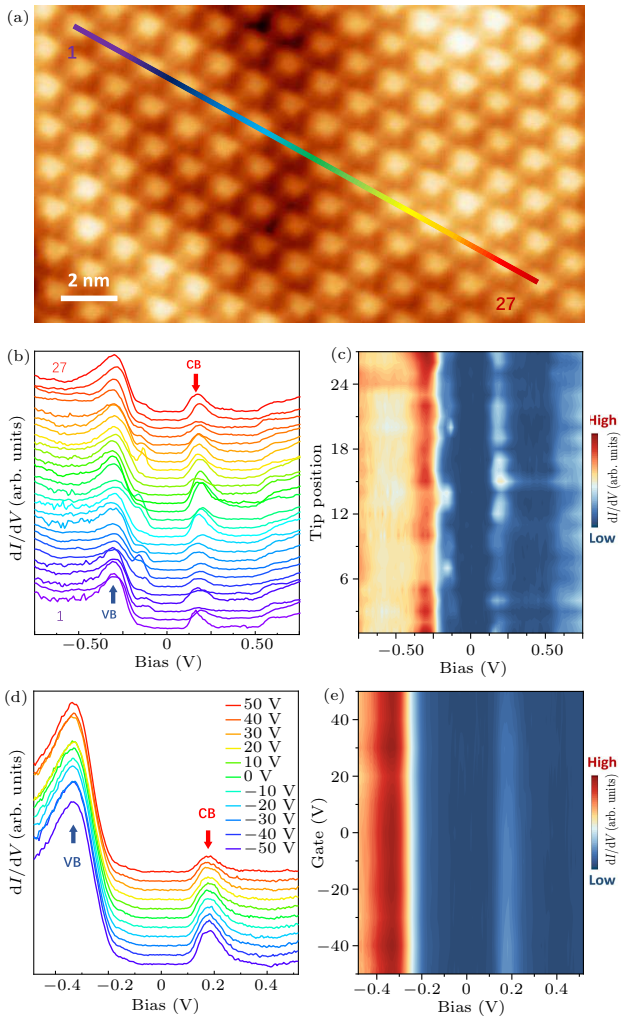



**Fig. 3.** Spatially resolved STS spectra and fixed-point gate response of monolayer $TaSe_2$. (a) STM topography of a monolayer $TaSe_2$ region. (b) Twenty-seven $dI/dV$ spectra acquired along the marked path in (a), showing the continuous evolution of local electronic states in real space. (c) Corresponding intensity plot, providing a direct visualization of spectral-weight evolution as a function of position and bias. (d) Gate-dependent fixed-point $dI/dV$ spectra measured in the monolayer region. The arrows in panels (b) and (d) mark the valence-band (VB) and conduction-band (CB) features. (e) Corresponding gate-bias intensity map.

The same monolayer region was then examined by fixed-point gate-dependent STS. The spectra in Fig. 3(d) and the corresponding gate-bias map in Fig. 3(e) show that the dominant spectral features remain nearly unchanged over the accessible gate range. This weak response is physically reasonable for at least two reasons. First, the monolayer is directly supported by graphene, whose mobile carriers provide strong

Thomas–Fermi screening of the back-gate electric field before it can efficiently modulate the local potential landscape of the $TaSe_2$ overlayer. Second, single-layer 1T-$TaSe_2$ is itself a robust Mott-like insulator with a relatively large low-energy gap and low electronic compressibility. Within the present gate-voltage window, the induced carrier variation is therefore likely insufficient to drive a sizable redistribution of states across the gap. Under the present device geometry and spectroscopic resolution, the monolayer response is thus best described as strongly suppressed rather than completely absent. This point is important because it provides a direct physical reference for the more pronounced bilayer response discussed below.

### 3.3. Zero-gate STM characterization in bilayer $TaSe_2$

In sharp contrast to the monolayer's weak gate response, bilayer $TaSe_2$ presents a distinctly different electronic landscape, starting with its richer zero-gate properties. Figure 4(a) collects bias-dependent STM topographies of bilayer $TaSe_2$ obtained over a wide energy window from $-1$ V to $+1$ V. Across this range, the spatial contrast evolves systematically with bias, while the FFT in each panel confirms that the periodic structure remains well defined. The sequence shows that the bilayer electronic structure is broadly energy dependent rather than confined to a narrow low-energy feature.

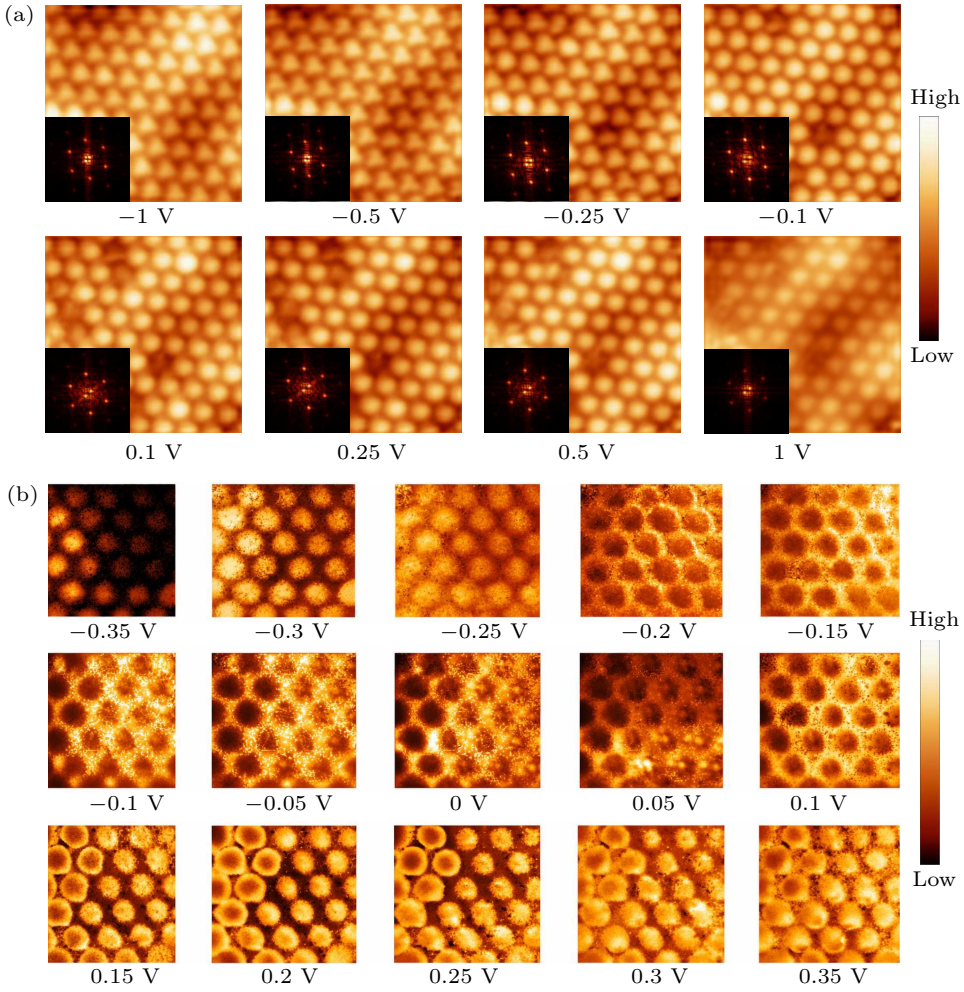



**Fig. 4.** STM and STS characterization of bilayer $TaSe_2$ at zero gate. (a) Bias-dependent STM spatial maps acquired with $I_{set} = 100$ pA (10 nm×10 nm); the insets display the FFT patterns, allowing direct comparison of the periodic structure at different energies. (b) $dI/dV$ mappings acquired with $I_{set} = 500$ pA (5 nm×5 nm), revealing the evolution of the charge-density-wave electronic structure of bilayer $TaSe_2$ near the Fermi level.

This behavior becomes more striking in the finer low-energy maps shown in Fig. 4(b), which cover $-0.35$ V to $+0.35$ V with small bias steps. The contrast evolves continuously across the Fermi-level region. On the negative-bias side, the structure is dominated by compact bright motifs. Closer to zero bias, the contrast becomes more ring-like and hollow-centred, whereas on the positive-bias side the bright motifs re-emerge with a modified intensity distribution. These maps establish that bilayer $TaSe_2$ hosts a bias-sensitive CDW electronic structure and provide the zero-gate context required to interpret the subsequent gate-dependent spectroscopy.

### 3.4. Gate-dependent local spectroscopy in bilayer $TaSe_2$

Having mapped the bias-dependent electronic structure at zero gate, we now apply back-gate tuning to quantify the local

electrostatic response of bilayer $TaSe_2$ and compare it directly with the monolayer case. Figure 5 presents the fixed-point gate response of the bilayer region. The atomically resolved topography in Fig. 5(a) identifies the measurement location, and the representative spectrum at $V_g = 0$ V in Fig. 5(b) provides the local spectral baseline. Figure 5(c) displays the spectra acquired at the same point under different back-gate voltages over the range from $-50$ V to $+50$ V. The interval was chosen because it provides stable tunnelling conditions and a representative electrostatic-tuning window for direct comparison in the present back-gated device. The valence-band (VB) and conduction-band (CB) features are marked by arrows in Figs. 5(b) and 5(c). Figure 5(d) summarizes the evolution as a gate-bias color map.

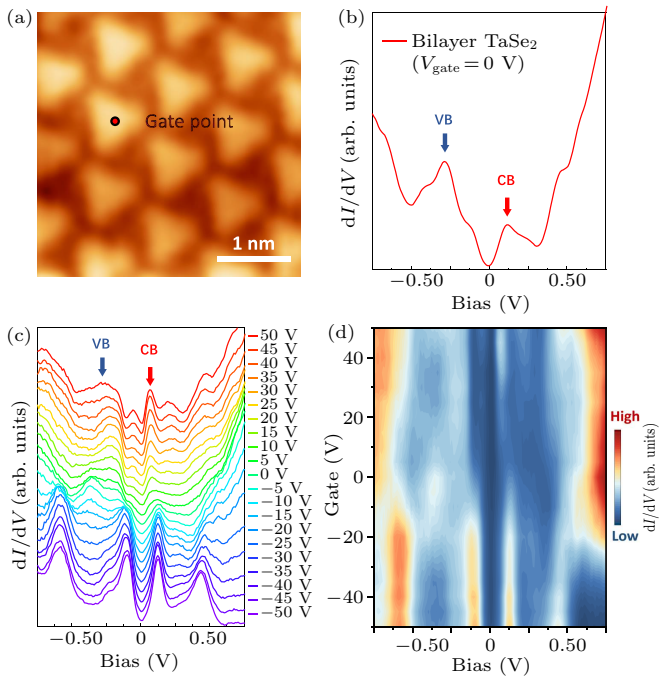



**Fig. 5.** Gate-tuned spectroscopy at a fixed point in bilayer $TaSe_2$. (a) STM topography of a bilayer region with the blue dot marking the position for gate-dependent measurements. (b) Representative $dI/dV$ spectrum acquired at this position at $V_g = 0$ V. (c) Gate-dependent $dI/dV$ spectra measured at the same point under back-gate voltages from $-50$ V to $+50$ V. The arrows in panels (b) and (c) mark the valence-band (VB) and conduction-band (CB) features. (d) Corresponding gate-bias color map. Compared with the monolayer region, bilayer $TaSe_2$ exhibits more pronounced spectral-weight redistribution and clearer low-energy feature evolution under the present experimental conditions, indicating stronger local sensitivity to back-gate tuning.

In contrast to the monolayer case, the bilayer spectra exhibit a clear gate dependence. The response is better described as a redistribution of spectral weight among selected low-energy and intermediate-energy features than as a rigid shift of the entire spectrum. Several nearly vertical features in the gate–bias map remain trackable across the full gate range, indicating that the bilayer's local density of states is measurably altered by the applied back gate. The comparison between Figs. 3 and 5 therefore establishes a layer-dependent local gate response: the monolayer remains nearly unchanged under the present conditions, whereas the bilayer shows a clearly resolvable spectral evolution. This contrast is consistent with the idea that the additional $TaSe_2$ layer weakens the strongly gapped, weakly compressible single-layer limit and makes the bilayer electronic structure more susceptible to electrostatic tuning. From a structural viewpoint, the extra $TaSe_2$ layer introduces additional interlayer hybridization and dielectric screening, which soften the low-energy electronic structure relative to the more weakly screened monolayer limit and make spectral weight easier to reorganize under gate tuning.

## 4. Conclusions

We have established a reliable gate-tunable STM platform for $TaSe_2$ films grown on graphene, and resolved the layer-dependent local gate response by combining atomic-resolution imaging, spatially resolved spectroscopy, bias-dependent mapping, and fixed-point gate-dependent STS. Monolayer $TaSe_2$ shows markedly suppressed gate response under the present measurement conditions, consistent with efficient electrostatic screening by the graphene substrate and the robust Mott-like correlated state in single-layer 1T-$TaSe_2$. In sharp contrast, bilayer $TaSe_2$ exhibits a much richer zero-gate CDW electronic structure and pronounced gate-induced spectral-weight redistribution over the back-gate range from $-50$ V to $+50$ V. These results suggest that layer thickness provides an effective knob to control the electrostatic responsiveness of correlated 2D materials. The framework can be further extended to superconducting or charge-ordered van der Waals systems such as Fe(Te,Se), $NbSe_2$ and related heterostructures, where local electrostatic tuning may help reveal new interfacial quantum states and guide the design of tunable quantum materials.

## Acknowledgements

The work is supported by the National Natural Science Foundation of China (Grant Nos. 12522408, 62488201, 61925111, U23A6015, 52572188, 12374199, and 52250402), the National Key Research and Development Program of China (Grant Nos. 2024YFA1207800 and 2025YFA1212800), CAS Project for Young Scientists in Basic Research (Grant No. YSBR-003), and the Beijing Nova Program (20240484651). This work also benefitted from the resources and support from the Electron Microscopy Center at the University of Chinese Academy of Sciences.

## References

[1] Novoselov K S, Geim A K, Morozov S V, Jiang D, Zhang Y, Dubonos S V, Grigorieva I V and Firsov A A 2004 *Science* **306** 666
[2] Novoselov K S, Geim A K, Morozov S V, Jiang D, Katsnelson M I, Grigorieva I V, Dubonos S V and Firsov A A 2005 *Nature* **438** 197
[3] Zhang Y, Tan Y W, Stormer H L and Kim P 2005 *Nature* **438** 201

[4] Geim A K and Grigorieva I V 2013 *Nature* **499** 419
[5] Hu J W, Zhu S Y, Hu Q Y, Wang Y H, Shen C M, Yang H T, Zhu X S, Hua Q, Xu Y and Gao H J 2024 *Chin. Phys. Lett.* **41** 037401
[6] Wang Q H, Kalantar-Zadeh K, Kis A, Coleman J N and Strano M S 2012 *Nat. Nanotechnol.* **7** 699
[7] Chhowalla M, Shin H S, Eda G, Li L J, Loh K P and Zhang H 2013 *Nat. Chem.* **5** 263
[8] Manzeli S, Ovchinnikov D, Pasquier D, Yazyev O V and Kis A 2017 *Nat. Rev. Mater.* **2** 17033
[9] Ye J T, Zhang Y J, Akashi R, Bahramy M S, Arita R and Iwasa Y 2012 *Science* **338** 1193
[10] Li L, Yu Y, Ye G J, Ge Q, Ou X, Wu H, Feng D, Chen X H and Zhang Y 2014 *Nat. Nanotechnol.* **9** 372
[11] Xia F, Wang H and Jia Y 2014 *Nat. Commun.* **5** 4458
[12] Tongay S, Sahin H, Ko C, Luce A, Fan W, Liu K, Zhou J, Huang Y S, Ho C H, Yan J, Ogletree D F, Aloni S, Ji J, Li S, Li J, Peeters F M and Wu J 2014 *Nat. Commun.* **5** 3252
[13] Chenet D A, Aslan B, Huang P Y, Fan C, van der Zande A M, Heinz T F and Hone J 2015 *Nano Lett.* **15** 5667
[14] Ali M N, Xiong J, Flynn S, Tao J, Gibson Q D, Schoop L M, Liang T, Haldolaarachchige N, Hirschberger M, Ong N P and Cava R J 2014 *Nature* **514** 205
[15] Wang X, Jones A M, Seyler K L, Tran V, Jia Y, Zhao H, Wang H, Yang L, Xu X and Xia F 2015 *Nat. Nanotechnol.* **10** 517
[16] Qiao J, Kong X, Hu Z X, Yang F and Ji W 2014 *Nat. Commun.* **5** 4475
[17] Wu W, Wang L, Li Y, Zhang F, Lin L, Niu S, Chenet D, Zhang X, Hao Y, Heinz T F, Hone J and Wang Z L 2014 *Nature* **514** 470
[18] Zhu H, Wang Y, Xiao J, Liu M, Xiong S, Wong Z J, Ye Z, Ye Y, Yin X and Zhang X 2015 *Nat. Nanotechnol.* **10** 151
[19] Hellmann S, Rohwer T, Kalläne M, Hanff K, Sohrt C, Stange A, Carr A, Murnane M M, Kapteyn H C, Kipp L, Bauer M and Rossnagel K 2012 *Nat. Commun.* **3** 1069
[20] Huber T, Mariager S O, Ferrer A, Schäfer H, Johnson J A, Grübel S, Lübcke A, Huber L, Kubacka T, Dornes C, Laulhe C, Ravy S, Ingold G, Beaud P, Demsar J and Johnson S L 2014 *Phys. Rev. Lett.* **113** 026401
[21] Brun C, Wang Z Z, Monceau P and Brazovskii S 2010 *Phys. Rev. Lett.* **104** 256403
[22] van Midden M A, van Midden H J P, Prodan A, Bennett J C and Zupanič E 2020 *Phys. Rev. B* **102** 075442
[23] Zhang H, Chen H, Huang Z, Wang Z A, Lv S, Xian G, Guo H, Yang H and Gao H J 2025 *Nano Lett.* **25** 16650
[24] Liu S, Nie S M, Qi Y P, Guo Y F, Yuan H T, Yang L X, Chen Y L, Wang M X and Liu Z K 2021 *Chin. Phys. Lett.* **38** 077302
[25] Chen W, Zhong H, Bao C, Wang F, Cai X, Yun C, Teng H, Wei Z and Zhou S 2025 *Chin. Phys. Lett.* **42** 017101
[26] Wang R, Ding J, Sun F, Zhao J and Qiu X 2024 *Chin. Phys. Lett.* **41** 057801
[27] Rossnagel K 2011 *J. Phys.: Condens. Matter* **23** 213001
[28] Chen Y, Ruan W, Wu M, Tang S, Ryu H, Tsai H Z, Lee R L, Kahn S, Liou F, Jia C, Albertini O R, Xiong H, Jia T, Liu Z, Sobota J A, Liu A Y, Moore J E, Shen Z X, Louie S G, Mo S K and Crommie M F 2020 *Nat. Phys.* **16** 218
[29] Ruan W, Chen Y, Tang S, Hwang J, Tsai H Z, Lee R L, Wu M, Ryu H, Kahn S, Liou F, Jia C, Aikawa A, Hwang C, Wang F, Choi Y, Louie S G, Lee P A, Shen Z X, Mo S K and Crommie M F 2021 *Nat. Phys.* **17** 1154
[30] Nakata Y, Sugawara K, Chainani A, Oka H, Bao C, Zhou S, Chuang P Y, Cheng C M, Kawakami T, Saruta Y, Fukumura T, Zhou S, Takahashi T and Sato T 2021 *Nat. Commun.* **12** 5873
[31] Hwang J, Ruan W, Chen Y, Tang S, Crommie M F, Shen Z X and Mo S K 2024 *Rep. Prog. Phys.* **87** 044502
[32] Nakata Y, Sugawara K, Shimizu R, Okada Y, Han P, Hitosugi T, Ueno K, Sato T and Takahashi T 2016 *NPG Asia Mater.* **8** e321
[33] Liu L, Yang H, Huang Y, Song X, Zhang Q, Huang Z, Hou Y, Chen Y, Xu Z, Zhang T, Wu X, Sun J, Huang Y, Zheng F, Li X, Yao Y, Gao H J and Wang Y 2021 *Nat. Commun.* **12** 1978
[34] Liu M, Leveillee J, Lu S, Yu J, Kim H, Tian C, Shi Y, Lai K, Zhang C, Giustino F and Shih C K 2021 *Sci. Adv.* **7** eabi6339
[35] Tu W, Lv R, Shao D, Sun Y and Lu W 2025 *Chin. Phys. B* **34** 097103
[36] Binnig G, Rohrer H, Gerber C and Weibel E 1982 *Phys. Rev. Lett.* **49** 57
[37] Tersoff J and Hamann D R 1985 *Phys. Rev. B* **31** 805
[38] Zhu T, Ruan W, Wang Y Q, Tsai H Z, Wang S, Zhang C, Wang T, Liou F, Watanabe K, Taniguchi T, Neaton J B, Weber-Bargioni A, Zettl A, Qiu Z Q, Zhang G, Wang F, Moore J E and Crommie M F 2022 *Nat. Mater.* **21** 748
[39] Qiu Z, Han Y, Noori K, Chen Z, Kashchenko M, Lin L, Olsen T, Li J, Fang H, Lyu P, Telychko M, Gu X, Adam S, Quek S Y, Rodin A, Castro Neto A H, Novoselov K S and Lu J 2024 *Nat. Mater.* **23** 1055
[40] Lowe B, Field B, Hellerstedt J, Ceddia J, Nourse H L, Powell B J, Medhekar N V and Schiffrin A 2024 *Nat. Commun.* **15** 3559
[41] Taheri M, Brown J, Rehman A, Sesing N, Kargar F, Salguero T T, Rumyantsev S and Balandin A A 2022 *ACS Nano* **16** 18968
[42] Shen S W, Qin T, Gao J J, Wen C H, Wang J H, Wang W, Li J, Luo X, Lu W J, Sun Y P and Yan S C 2022 *Chin. Phys. Lett.* **39** 077401
[43] Li Y, Xiao Y, Zheng Q, Lin X, Huang L and Gao H J 2023 *Chin. Phys. B* **32** 077101
[44] Zong J, Xie Y, Meng Q, *et al.* 2022 *Chin. Phys. B* **31** 107301
[45] Xie X D, Lin D J, Zhu L, Li Q Y, Zong J Y, Chen W, Meng Q H, Tian Q C, Li S C, Xi X, Wang C and Zhang Y 2021 *Chin. Phys. Lett.* **38** 107101
[46] Fan J Z, Fang Z B, Luo C J and Zhang H 2022 *Acta Phys. Sin.* **71** 127103 (in Chinese)
[47] Feng H, Li Y, Shi Y, Xie H Y, Li Y Q and Xu Y 2022 *Chin. Phys. Lett.* **39** 077501
[48] Wang Y D, Yao W L, Xin Z M, Han T T, Wang Z G, Chen L, Cai C, Li Y and Zhang Y 2020 *Nat. Commun.* **11** 4215
[49] Xi X, Wang Z, Zhao W, Park J H, Law K T, Berger H, Forró L, Shan J and Mak K F 2016 *Nat. Phys.* **12** 139
[50] Koma A 1992 *Thin Solid Films* **216** 72
[51] Mañas-Valero S, Huddart B, Lancaster T, Coronado E and Pratt F 2021 *npj Quantum Mater.* **6** 69
[52] Cho D, Cheon S, Kim K S, Lee S H, Cho Y H, Cheong S W and Yeom H W 2016 *Nat. Commun.* **7** 10453
[53] Cho D, Gye G, Lee J, Lee S H, Wang L, Cheong S W and Yeom H W 2017 *Nat. Commun.* **8** 392
[54] Park J W, Lee J and Yeom H W 2021 *npj Quantum Mater.* **6** 32